remote sensing

MDPI

Article

Vegetation Growth Response and Trends after Water Deficit Exposure in the Loess Plateau, China

Yuanyuan Luo [1], Wei Liang [1,2], Jianwu Yan [1,2,*], Weibin Zhang [3], Fen Gou [1], Chengxi Wang [1] and Xiaoru Liang [1]

[1] School of Geography and Tourism, Shaanxi Normal University, Xi'an 710119, China
[2] National Demonstration Center for Experimental Geography Education, Shaanxi Normal University, Xi'an 710119, China
[3] College of Water Resources and Architectural Engineering, Northwest A&F University, Xianyang 712100, China
* Correspondence: yanjw@snnu.edu.cn; Tel.: +86-029-85310525

Abstract: Understanding the impact of water availability on vegetation growth in the context of climate change is crucial for assessing the resilience of vegetation to environmental shifts. In this study, the relationship between vegetation growth and water availability was studied using a variety of indicators. The Normalized Difference Vegetation Index (NDVI), the Enhanced Vegetation Index (EVI), and Solar-Induced Chlorophyll Fluorescence (SIF) were utilized as vegetation growth indicators, while the standardized precipitation evapotranspiration index (SPEI) and soil moisture indicators served as water use indices. To investigate the vegetation response to water deficit in the Loess Plateau during the growing season from 2000 to 2020, Spearman's rank correlation coefficients were calculated using a 5-year sliding window approach. The spatial and temporal heterogeneity of vegetation response to water deficit during the growing seasons were also explored. The results showed that: (1) with the improvement of moisture conditions, vegetation growth recovered significantly, and there was no expansion trend for vegetation water deficit. (2) The most sensitive timescale of vegetation to water deficit was 6–8 months; the response degree and sensitivity of vegetation to water surplus and deficit were the highest from June to August; and broadleaved forest was the vegetation type most sensitive to water deficit in the early growing season, while grass was the vegetation type most sensitive to water deficit during the mid and late growing seasons. (3) Soil moisture emerged as the dominant factor influencing vegetation growth in the Loess Plateau, followed by precipitation, albeit to a lesser extent. These findings contribute to understanding the mechanism and characteristics of the response of vegetation to climate fluctuations induced by global climate change.

Keywords: Loess Plateau; NDVI; SPEI; water deficit; multiple timescales; water availability

Citation: Luo, Y.; Liang, W.; Yan, J.; Zhang, W.; Gou, F.; Wang, C.; Liang, X. Vegetation Growth Response and Trends after Water Deficit Exposure in the Loess Plateau, China. *Remote Sens.* **2023**, *15*, 2593. https://doi.org/10.3390/rs15102593

Academic Editors: Hooman Latifi, Nikos Koutsias and Hamed Naghavi

Received: 16 March 2023
Revised: 3 May 2023
Accepted: 9 May 2023
Published: 16 May 2023

1. Introduction

As global warming intensifies, extreme weather and climate events are becoming more frequent [1]. These events include cumulative water deficit events, which seriously threaten terrestrial ecosystems and human societies, making water deficit an increasingly prominent global issue [2]. Extreme droughts, in particular, have the potential to alter the carbon balance of terrestrial ecosystems and may cause them to transition from carbon sinks to carbon sources [3]. This carbon–climate feedback effect can lead to increased droughts and the irreversible degradation of ecosystems [4–6]. However, different terrestrial ecosystems respond to climate change in different ways [7], and the response of vegetation growth to drought exhibits significant spatiotemporal heterogeneity [8]. Under drought conditions, vegetation experiences water stress, which causes stomata to close and reduces the rates of photosynthesis, leading to a decline in primary productivity [9]. Consequently, drought can result in a growth slowdown, degradation, or even death of the vegetation [10,11]. Therefore, studying the vegetation response to drought is crucial to understanding the

underlying mechanisms and characteristics of vegetation response to climate variability in the context of global climate change [3].

The relationship between drought and vegetation has been extensively explored [8,12,13]. Drought is essentially characterized by a water deficit event, and the vegetation's response to such events is not always straightforward, as plant species exhibit different levels of resistance and resilience to water deficit due to their unique physiological responses [14,15]. The physiological characteristics of vegetation are mainly influenced by the climatic conditions of the different vegetation types in various climatic zones [16]. Moreover, the response of vegetation to drought is affected by drought characteristics and climatic environments [17], making it a complex process influenced by many eco-physiological and climatic factors [18,19]. To precisely monitor the overall climate condition and depict the temporal and spatial distribution of drought, a drought index that synthesizes the effects of temperature, precipitation, and radiation on vegetation is imperative [20]. These indices, such as the Moisture Index (MI) [21], the Palmer Drought Severity Index (PDSI) [22], the Standardized Precipitation Index (SPI) [23], and the Standardized Precipitation Evapotranspiration Index (SPEI) [19], are widely used and have been found to be well-correlated with vegetation indicators such as the NDVI, EVI, the Leaf Area Index (LAI), and Gross Primary Productivity (GPP) [24]. Notably, the SPEI holds an advantage over other drought indicators as it combines potential evapotranspiration and precipitation data to gauge the severity of drought [19]. Furthermore, it can indicate drought conditions at different timescales [25]. The timescale of drought, which refers to the duration from the onset of vegetation water deficit (VWD) to the determination of vegetation change, has been widely used in aridification studies [5,8,26].

Vegetation growth responses to climate change have been widely studied at global and regional levels. However, the effects of water limitation on vegetation growth in arid and semi-arid areas and how they will respond to climate change remain to be thoroughly explored. The Loess Plateau is particularly susceptible to frequent droughts caused by climate warming, which has had an increasing impact on vegetation [27]. The moisture required for vegetation growth in this region mainly comes from soil moisture, which is unevenly distributed due to the deep soil layer and buried groundwater [28]. Although existing studies have employed statistical analyses and vegetation indices to characterize the spatial and temporal variation in the response of regional vegetation to water surplus and deficit, the sensitivity of vegetation to changes in water deficit and how vegetation will adapt to or resist climate changes is not clear [29]. Furthermore, there are fewer studies regarding the impact of seasonal drought on land surface dynamics, and many uncertainties still need to be investigated regarding vegetation sensitivity to seasonal drought at the regional scale [13]. Therefore, a more comprehensive study of the effects of drought and climate change on vegetation in arid and semi-arid regions, such as the Loess Plateau, is necessary to develop strategies for the sustainable management of land and water resources.

The objective of this study is to investigate the expanding trend of increasing vegetation water deficit in regards to climate change across diverse climatic zones, as well as the response mechanisms of vegetation to water deficit in these zones. The study aimed to achieve the following goals: (1) investigate the expansion trend of VWD in various climatic zones; (2) analyze the characteristics of the response of vegetation to water deficit from three perspectives, namely, different climatic zones, growing season stages, and vegetation types; (3) attempt to explain the reasons behind the variations in the expansion trend of VWD among different climatic zones based on the above perspectives; and (4) identify future sustainable changes in vegetation and moisture conditions and investigate the environmental factors that govern vegetation growth. Our study aims to comprehensively assess the resistance and resilience of vegetation to drought and its potential risks to vegetation health. Furthermore, the study intends to establish a foundation for formulating and implementing measures to alleviate vegetation drought.

2. Materials and Methods

2.1. Study Area

The Loess Plateau, located between 33°43′–41°16′N and 100°54′–114°33′E, encompasses most of Shaanxi, Shanxi, and Ningxia, as well as parts of Qinghai, Gansu, Henan, and Inner Mongolia. It covers an area of approximately 620,000 km^2 in the middle reaches of the Yellow River [13] (Figure 1). The region is known for severe soil erosion and the most fragile ecology, with an arid continental monsoon climate [30]. Precipitation in the Loess Plateau is low and unevenly distributed in time and space, and it is concentrated from June to September, primarily in heavy rainfall. The average annual precipitation is 150 mm·a^{-1} to 800 mm·a^{-1}, decreasing from northwest to southeast [31]. The growing season occurs from April-October, accounting for about 92.00% of the annual precipitation [32]. In consideration of the Loess Plateau's climatic attributes, this paper divides it into three distinct climatic zones: arid, semi-arid, and semi-humid [33], representing 13.13%, 62.98%, and 23.99% of the total area, respectively. The research primarily focuses on examining the spatiotemporal heterogeneity of the response of vegetation growth to water availability during the growing season from 2000 to 2020.

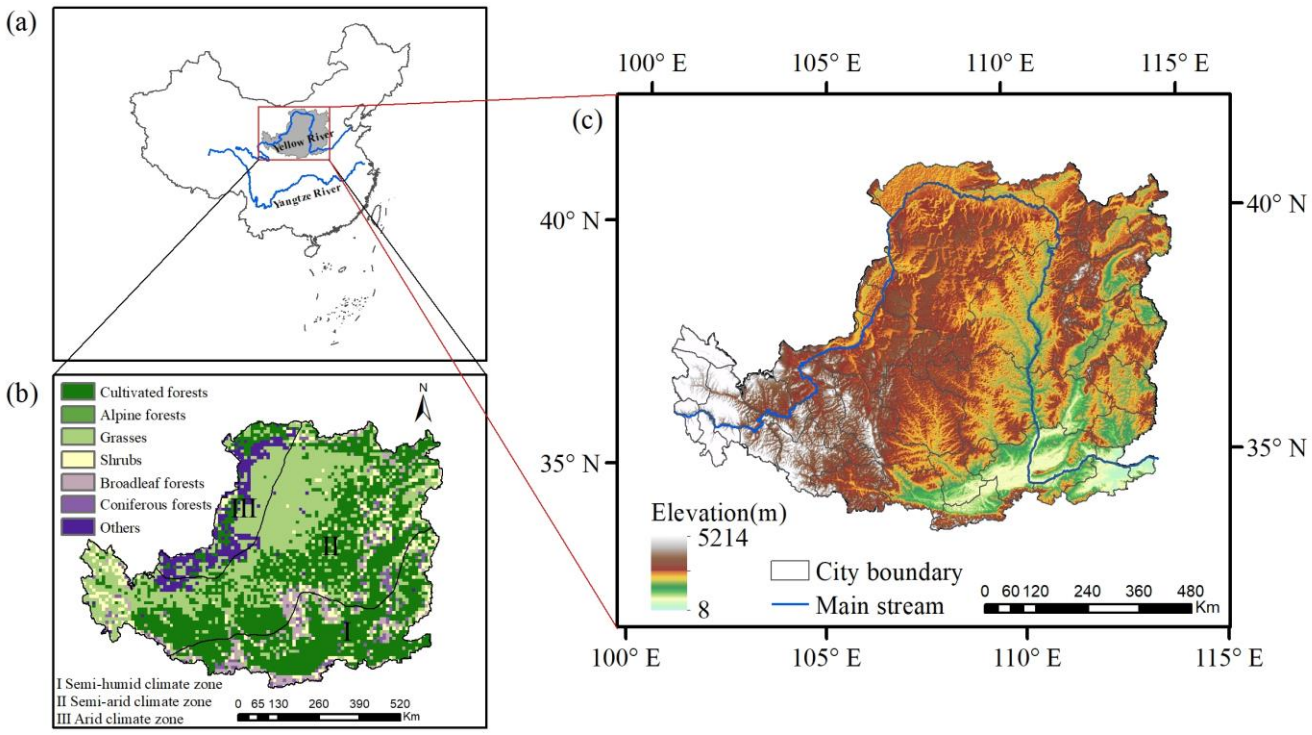

Figure 1. Background information on the study area: (**a**) location; (**b**) vegetation cover type data; and (**c**) elevation.

2.2. Data Sources

2.2.1. Meteorological Data

The monthly precipitation dataset and the monthly mean temperature dataset, with 1 km resolution, were provided by the National Earth System Science Data Center, National Science and Technology Infrastructure of China (http://www.geodata.cn, accessed on 11 May 2022). The precipitation and temperature datasets were generated by the delta spatial downscaling scheme in the Chinese region, based on the global 0.5° climate data released by CRU and the global high-resolution climate data released by WorldClim. The accuracy and reliability of the datasets were verified by comparing them with data from 496 independent meteorological observation stations, and the validation results were credible [34]. Monthly temperature and precipitation data from 1999 to 2020 were utilized to calculate SPEI to examine the meteorological changes and assess the response of vegetation

to varying durations of water deficit. To facilitate the calculation, the spatial resolution of all data was uniformly resampled to 0.1° for this study.

2.2.2. Soil Moisture

Soil moisture directly impacts vegetation growth and resistance to drought [35,36]. The Global Land Evaporation Amsterdam Model (GLEAM) was employed to provide the surface and root-zone soil moisture statistics used in this study [37,38]. The reliability of GLEAM soil moisture data has been verified by on-site soil moisture measurements in the Loess Plateau [39]. The 2000 to 2020 monthly surface soil moisture (0–10 cm) (SMsurf) and root-zone soil moisture (10–100 cm) (SMroot) data in GLEAM (v3.5a) were selected for analysis. Soil moisture is the primary source of water required for vegetation growth, and it determines the amount of water used by the vegetation [35]. As soils of different textures have varying water-holding capacities and nutrients [40–42], this study utilized soil moisture and SPEI at different timescales as water availability indicators.

2.2.3. Vegetation Indices

Two different vegetation indices, namely NDVI and EVI, were employed in this study. NDVI was selected, as it is widely used to assess vegetation status at regional and global levels. It is related to the vegetation canopy structure and coverage, as well as the photosynthesis of the vegetation canopy [43,44]. On the other hand, EVI was calculated by incorporating the light blue band of the spectrum, which mitigated the influence of the atmospheric and canopy background and enhanced the sensitivity in areas with a dense biomass [45]. Monthly NDVI and EVI data were obtained from moderate resolution imaging spectroradiometer (MODIS) product data (MOD13C2, V6).

2.2.4. Solar-Induced Chlorophyll Fluorescence (SIF)

Solar-induced chlorophyll fluorescence was selected for comparison with NDVI and EVI data, as it provided a signal corresponding to vegetation photosynthesis and was a more accurate assessment of the actual photosynthetic state of the vegetation than were traditional indices [46,47]. Integrating SIF with traditional vegetation indices provided a comprehensive analysis of vegetation status, enabling the dynamic monitoring of vegetation growth changes. A global, OCO-2-based SIF dataset (GOSIF) was generated by a machine learning approach based on discrete OCO-2 SIF soundings, remote sensing data from the MODIS, and meteorological reanalysis data through a data-driven approach [48].

2.2.5. Vegetation Cover Type Data

To investigate the variation in the expansion trend of VWD among different climatic zones, this study analyzed the characteristics of the responses of different vegetation types to water deficit. Vegetation cover types were acquired from the Data Center for Resources and Environmental Sciences, Chinese Academy of Sciences (http://www.resdc.cn, accessed on 1 October 2022) in May 2001. The vegetation types were extracted and categorized into six distinct cover types: grasses, shrubs, alpine forests, cultivated forests, broadleaved forests, and coniferous forests (Figure 1) (Table S1).

2.3. Standardized Precipitation Evapotranspiration Index

SPEI was proposed by Vicente-Serrano et al. [19]. The calculation of SPEI was based on monthly precipitation and temperature and was characterized by multiple timescales. SPEI's central concept is the construction of a meteorological water cycle to describe the accumulated water deficit or surplus, which can then be used to characterize drought [49]. High to low SPEI means relatively wet to relatively dry [50]. In this study, SPEI was calculated separately on 1–12 month timescales to assess the different durations of the water deficit. The specific calculation method for SPEI is given below.

First, Thornthwaite's method was employed to estimate the monthly potential evapotranspiration (PET_j, mm):

$$PET_j = 16K\left(\frac{10T_j}{I}\right)^m \tag{1}$$

where T_j is the monthly temperature of j; °C; I is the annual heat index, which is the sum of 12 monthly index values; m is the coefficient, depending on I; $m = 0.492 + 1.79 \times 10^{-2}I - 7.71 \times 10^{-5}I^2 + 6.75 \times 10^{-7}I^3$; and K is the correction factor for the latitude and month functions.

The accumulated moisture deficit sequence X, with different timescales, was constructed and its probability distributions were calculated. A month's cumulative moisture deficit is the sum of the previous $k-1$ months and the current month's moisture deficit, and k is the timescale, $k = 1, \cdots, 12$.

$$X_i^k = \sum D_i \tag{2}$$

$$D_i = P_i - PET_i \tag{3}$$

where P_i is the monthly precipitation (mm), D_i is the monthly moisture deficit (mm), and $i = 1, \cdots, n$, n is the number of samples in a time series. The calculation of the probability distribution function of the cumulative water deficit series is performed by introducing a three-parameter logarithm-logistics probability distribution function.

$$f(x) = \frac{\beta}{\alpha}\left(\frac{x-\gamma}{\alpha}\right)^{\beta-1}\left[1 + \left(\frac{x-\gamma}{\alpha}\right)^{\beta}\right]^{-2} \tag{4}$$

$\alpha, \beta,$ and γ are the scale, shape, and position parameters, respectively, for the D values in the range ($\gamma < D < \infty$). The probability distribution function of D is given according to the log-logistic distribution.

$$F(x) = \left(1 + \left(\frac{\alpha}{x-\gamma}\right)^{\beta}\right)^{-1} \tag{5}$$

Finally, SPEI was obtained as the standardized value of $F(x)$.

$$SPEI = W - \frac{c_0 + c_1W + c_2W^2}{1 + d_1W + d_2W^2 + d_3W^3} \tag{6}$$

$$W = \sqrt{-2\ln(P)} \tag{7}$$

For $P \leq 0.5$, P is the probability of exceeding the defined D value, $P = 1 - F(x)$. If $P > 0.5$, P is replaced by $1 - P$ and the resultant SPEI is the opposite; c_0, c_1, c_2, d_1, d_2 and d_3 are constants.

2.4. Trend Analysis

The Theil–Sen median method and the Mann–Kendall nonparametric statistical test were used to analyze the changes in vegetation growth, water availability, and meteorological elements in the Loess Plateau from 2000 to 2020. The trend is estimated as follows.

$$\beta = Median\left(\frac{X_j - X_i}{j-i}\right) \forall j > x \tag{8}$$

where β is the trend of change; i and j represent the time sequence; and X_i and X_j represent the values at moments i and j, respectively. $\beta > 0$ means an increasing trend, and $\beta < 0$ means a decreasing trend. The Mann–Kendall method was used to determine the significance of the trend, and Z values greater than 1.64 and 2.32 represent passing the significance tests with 95.00% and 99.00% confidence levels, respectively.

2.5. Spearman's Rank Correlation Coefficient

The Spearman's rank correlation is a distribution-independent measure of the strength of the association between variables. Compared with the Pearson correlation, this method is less sensitive to outliers. It does not rely on assumptions of normality or equal variance in variable distributions, so it is usually more widely applicable. The Spearman's rank correlation coefficient is calculated as follows:

$$\rho = 1 - \frac{6\sum d_i^2}{n(n^2-1)} \tag{9}$$

where ρ is the Spearman rank correlation coefficient; d_i is the difference in rank of the corresponding variables, i.e., the difference in rank of the variables in pairs after the two variables are sorted separately; and n is the number of observations.

2.6. Hurst Index Based on R/S Analysis

The Hurst index is a valuable tool for predicting the future evolution trend of the time series. It is based on the rescaled extreme deviation analysis (R/S) method, which takes values from 0 to 1, where a value of 0.5 indicates that the time series is randomly wandering. A value between 0 and 0.5 indicates an inverse time series persistence, while a value between 0.5 and 1 indicates a positive persistence of the time series [51–53]. This study classified the Hurst index into six categories based on the range of H values, $0 < H < 0.2$, $0.2 < H < 0.35$, $0.35 < H < 0.5$, $0.5 < H < 0.65$, $0.65 < H < 0.75$, and $H > 0.75$, which represents strong anti-sustainability, medium anti-sustainability, weak anti-sustainability, weak sustainability, medium sustainability, and strong sustainability, respectively. The results of the trend and the Hurst index calculations were combined and analyzed using cluster analysis to obtain different scenarios regarding the sustainability of a given factor over the coming years.

2.7. Standard Regression Coefficient Method

The standard regression coefficient method was used to calculate the standard coefficient of NDVI with respect to four meteorological factors, namely temperature, precipitation, soil moisture, and net solar radiation, on a raster basis. This allowed us to determine the contribution or relative importance of the inter-annual variation of NDVI. The variable with the highest absolute value of the standard regression coefficient was considered the dominant variable of the dependent variable in the grid. The calculation equation is used as follows.

$$\widetilde{NDVI}_k = a \times \widetilde{T}_k + b \times \widetilde{P}_k + c \times \widetilde{SM}_k + d \times \widetilde{Rad}_k \tag{10}$$

$$CR_a = \frac{|a|}{|a| + |b| + |c| + |d|} \tag{11}$$

where $\widetilde{T}_k$, $\widetilde{P}_k$, $\widetilde{SM}_k$, and $\widetilde{Rad}_k$ represent the standardized values of the growing season average NDVI, air temperature, precipitation, root-zone soil moisture, and net solar radiation in year k, respectively; CR_a represents the contribution of air temperature to the interannual variation of NDVI, and the contribution of precipitation, root-zone soil moisture, and net solar radiation were calculated using the same method.

3. Results

3.1. Trends in the Vegetation Growth and Moisture Conditions

3.1.1. Expansion Trend of VWD

The robustness of the calculated SPEIs was verified by comparing them with the SPEI of the SPEIbase v2.5 products, and the results showed that the SPEI index calculated in this study was reliable (Figures S1 and S2). To investigate the correlation between NDVI and cumulative water deficit events on different timescales during the 2000–2020 growing season, the 5-year sliding window was employed to calculate the Spearman's rank. Additionally, the correlation between NDVI and soil moisture was also compared. The area with a significant positive correlation area ($p < 0.05$) represents the VWD area, indicating that vegetation growth is promoted by an increase in water, while the areas with a significant negative correlation ($p < 0.05$) represent excess water, indicating that vegetation growth is inhibited by an increase in water. No significant correlation indicates that vegetation growth is not affected by water in the area [53]. Figure 2 displays inconsistent trends of water deficit or water surplus area obtained at short timescales, whereas those calculated at timescales greater than 6 months are more consistent (Figure 2d–f). The relevant literature also suggested that short timescales were unsuitable for arid and semi-arid areas such as the Loess Plateau [3,49,54,55]. Therefore, this study focused on the response characteristics of cumulative water deficit events with vegetation growth timescales greater than 6 months.

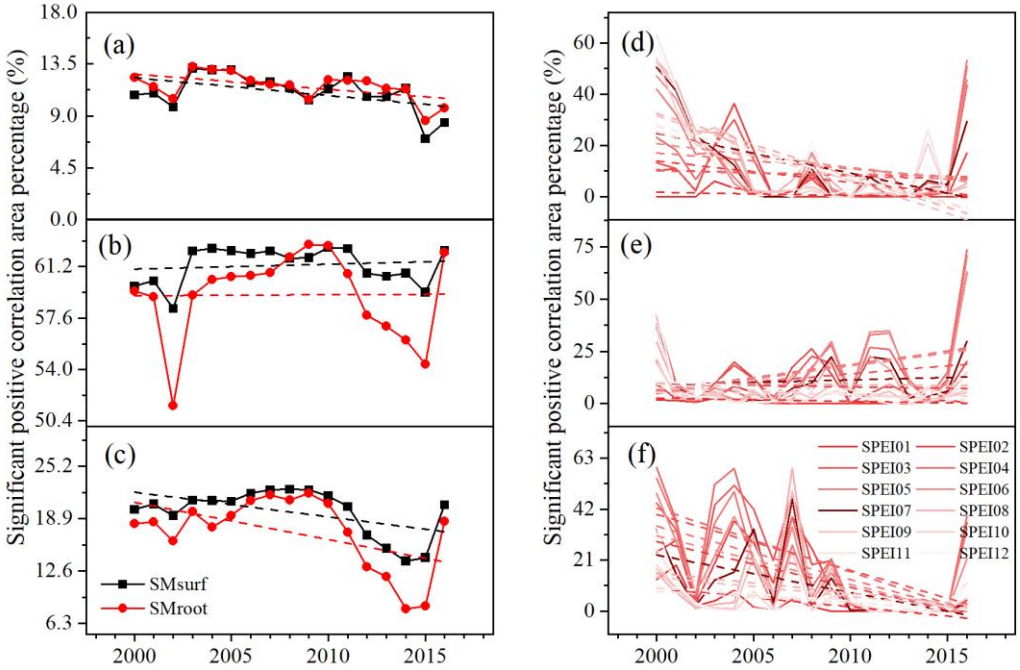

Figure 2. Area expansion trend of VWD in different climatic zones: (**a**–**c**) are the trends of VWD in arid, semi-arid, and semi-humid climate zones obtained by statistical analysis of the correlation between NDVI and SM, respectively; (**d**–**f**) are the trends of VWD in arid, semi-arid, and semi-humid climate zones obtained by statistical analysis of the correlation between NDVI and SPEI07, respectively. The major scale of the coordinate axis represents the starting year of the slide.

The VWD area in the Loess Plateau exhibited a decreasing trend ($p > 0.05$), which may be confounded by inconsistent regional results. Conversely, the vegetation water surplus area demonstrated an expanding trend ($p < 0.05$), which may be attributed to the increasing annual precipitation. During 2000–2020, the maximum percentage of vegetation surplus area was 1.75%, and the maximum VWD area was 16.06%. Given the small area of vegetation water surplus in the Loess Plateau, this study focuses on the VWD. As depicted in Figure 2, the trend of VWD area varied across different climate zone, and the changes in VWD and vegetation water surplus area were analyzed using the SPEI07

(7-month cumulative water balance), which yielded results consistent the soil moisture and NDVI. Thus, SPEI07 proves to be a suitable tool for examining the response of vegetation growth to water deficit in the Loess Plateau. From a regional perspective, the VWD in arid and sub-humid climate zones exhibited a decreasing trend, while the VWD in the semi-arid climate zone showed no significant increase. The vegetation recovery areas were primarily located in the semi-arid climate zone, implying that vegetation growth contributed to the expansion of water deficit areas. In terms of temporal changes, nearly all correlation coefficients that passed the significance test were positive. The distribution of the VWD areas varied significantly across different periods (Figure 3), with notable differences between the two periods requiring separate analysis and comparison with various natural factors, particularly the average water conditions in each period.

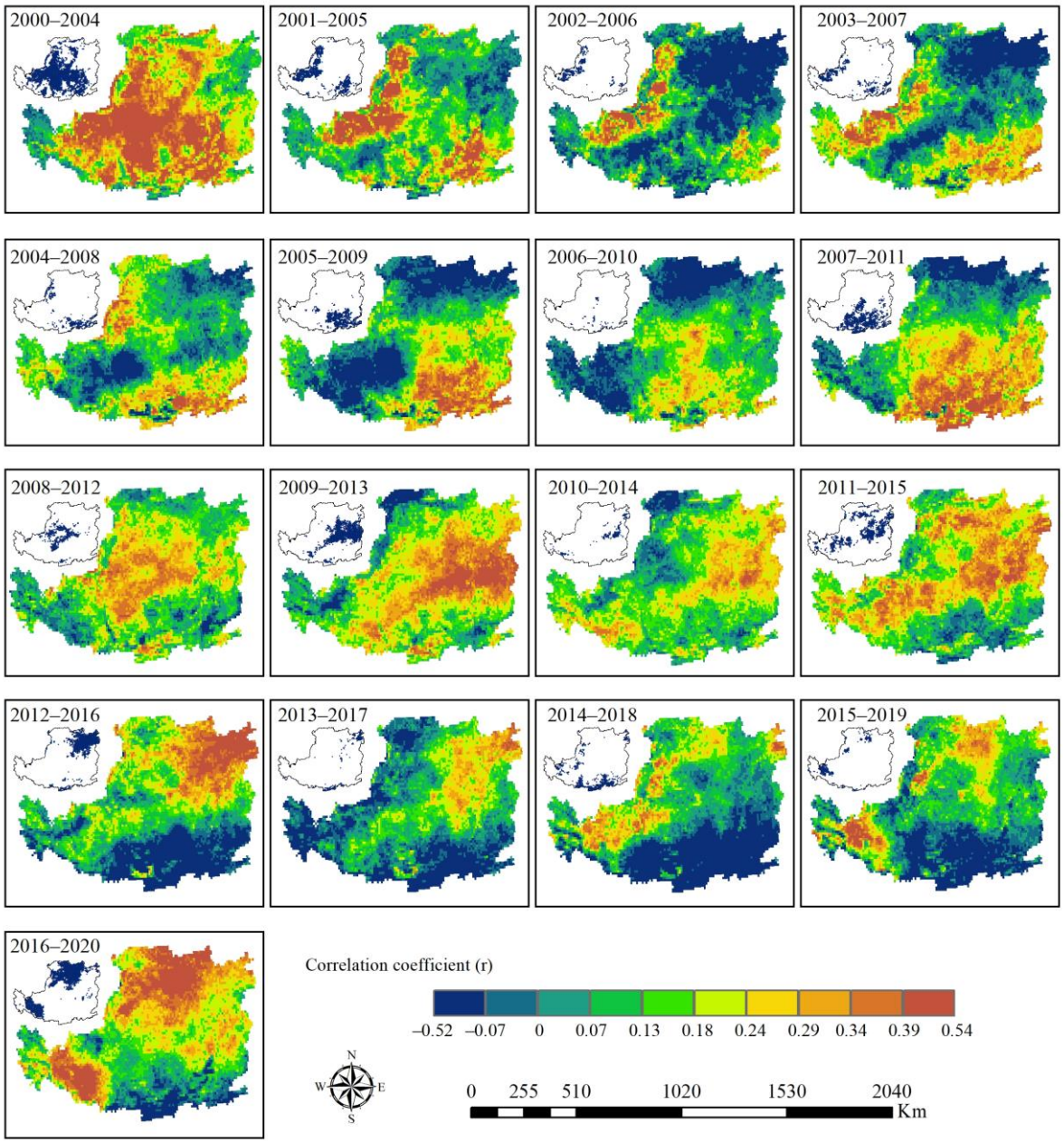

Figure 3. Correlation coefficients between NDVI and SPEI07 for the period of 2000–2020, calculated with a sliding window of 5 years. The top left graph represents the areas that passed the significance test ($p < 0.05$).

Based on the Spearman's rank correlation analysis of NDVI and SPEI07 from 2000 to 2020 (as depicted in Figure 4), it was observed that the total VWD area accounted for 38.31% during 2000–2020. In particular, vegetation growth in the northwestern and central parts of the Loess Plateau was significantly constrained by water deficit, whereas in other areas, vegetation was either not limited, or not significantly limited, by water surplus and deficit (Figure 4a–d). Of the VWD area, which accounted for 38.31%, 23.67% was situated in the semi-arid climate zone, 7.94% in semi-humid climate zone, and 6.70% in the arid climate zone. Since soil moisture is the primary source of moisture for vegetation growth, the correlation between the vegetation index and soil moisture is more significant. Accordingly, there are more regions with a significant positive correlation between NDVI and surface soil moisture, accounting for 90.66% of the total area. From southwest to northeast, there was a gradual increase in the degree of correlation. The less significant regions were mainly located in the southern Loess Plateau.

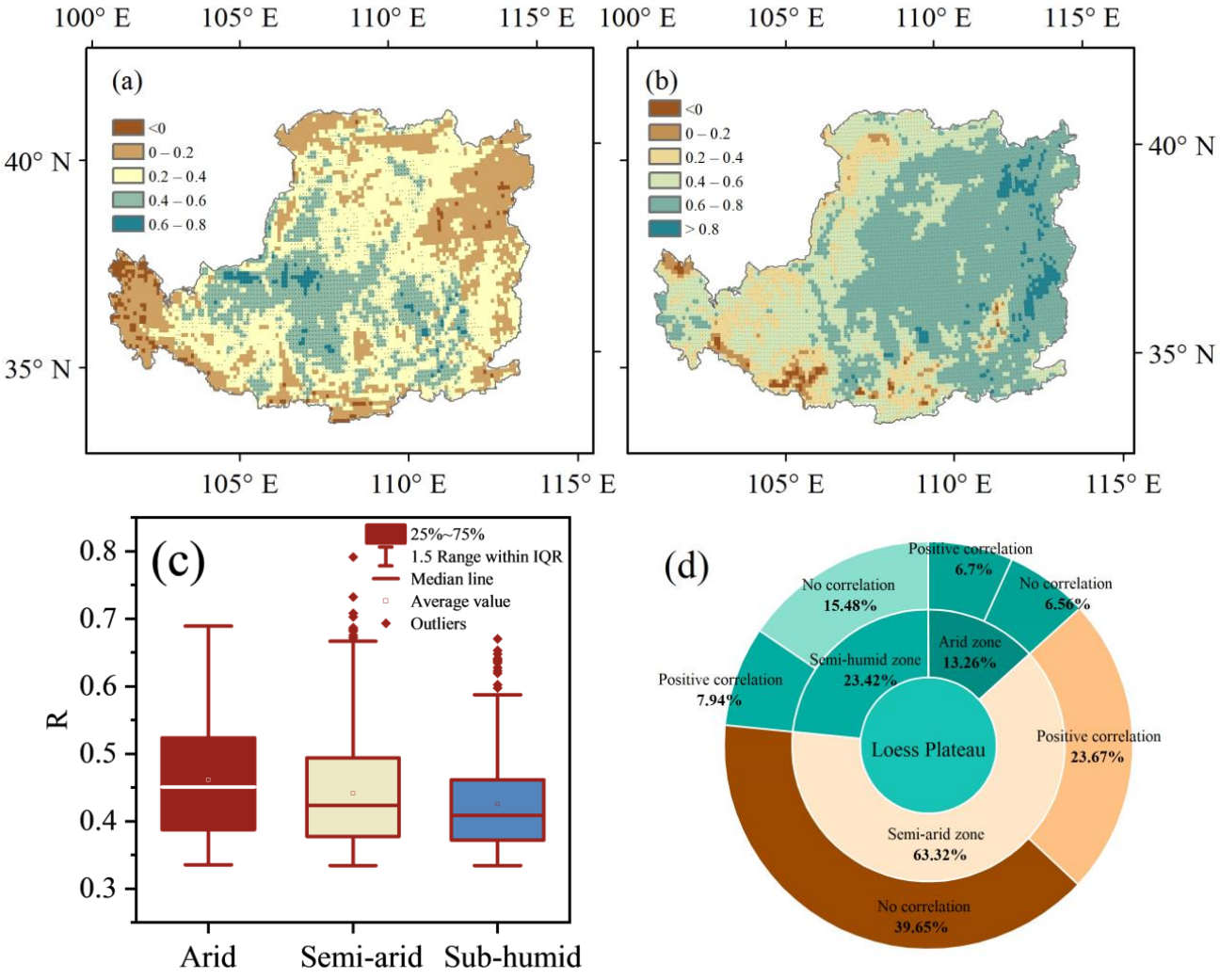

Figure 4. Spatial distribution of Spearman's correlation coefficients between the NDVI and the water availability index during the growing season from 2000 to 2020: (**a**,**b**) indicate the spatial distribution of the Spearman's correlation coefficients of NDVI with SPEI07 and SM, respectively; the black dots indicate a significant Spearman's correlation at $p < 0.05$; (**c**,**d**) indicate the correlation coefficients and significance distributions of NDVI and SPEI07 in the climate zones.

3.1.2. Trends of the Vegetation Growth Index, the Water Availability Index, and the Meteorological Index

Time trends were analyzed after standardizing the parameters with the min-max normalization. During the growing season, the vegetation area with an increasing trend (improvement area) accounted for 98.59%, while the decreasing trend (degradation area) accounted for only 1.41%. The Hurst index of annual mean growing NDVI was 0.46 on average, with 68.71% of the area exhibiting an index of less than 0.50, indicating that the NDVI changes were largely inversely persistent, with only a few areas being persistent. All three vegetation indices indicated that the vegetation cover increased during the growing seasons from 2000 to 2020, and the spatial distribution characteristics were consistent. In terms of the growth rate of the multi-year average growing season, NDVI showed a higher growth rate than EVI and SIF (Figure 5a–c). Figure 6 illustrates that the vegetation coverage rate in the Loess Plateau was low in the northwest and high in the southeast. The greening of vegetation was the most significant in the semi-humid climate zone, followed by the semi-arid climate zone, and was the least pronounced in the arid climate zone. The growth rate of vegetation cover in the semi-humid and semi-arid climate zone was similar, while it was the slowest in the arid climate zone. In arid and sub-humid climates, the average annual growing period regarding soil moisture and precipitation showed a downward trend, indicating vegetation degradation. In contrast, in semi-arid regions, the average annual growing period regarding soil moisture and precipitation increased, leading to significant improvement in vegetation (Figure 6). These findings suggest that vegetation growth is closely related to precipitation and soil moisture.

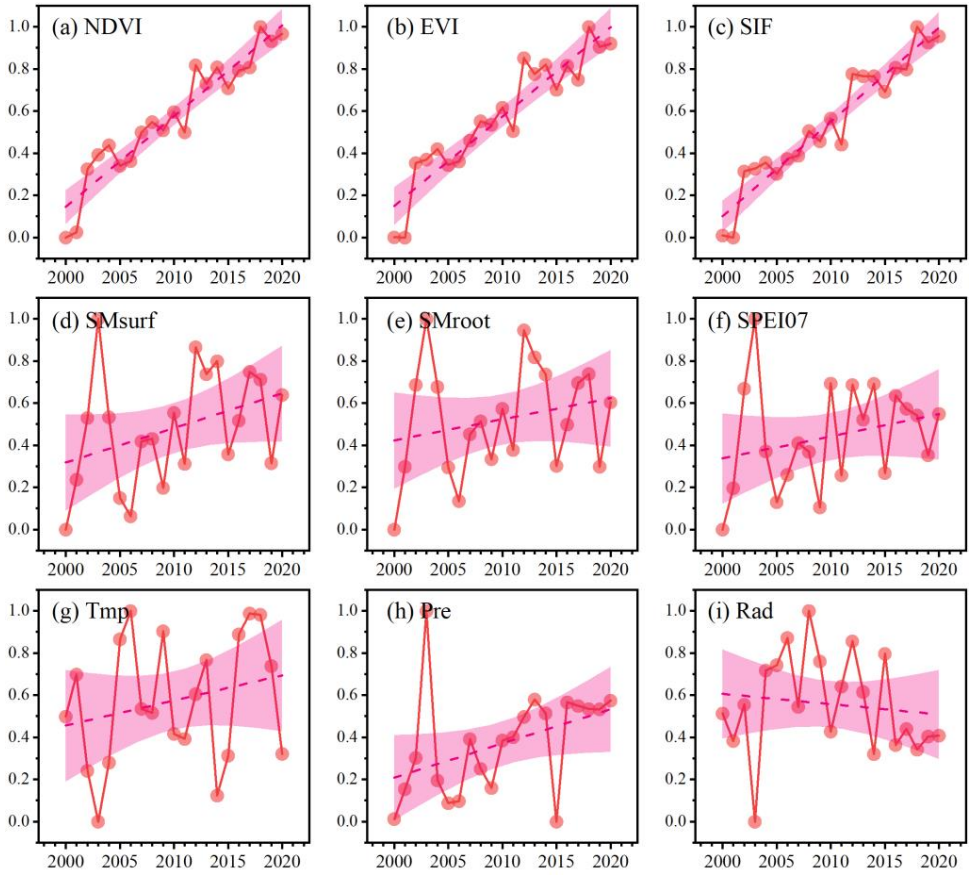

Figure 5. The annual trend of different standardized indices during the growing period from 2000 to 2020. The solid lines in (**a**–**i**) indicate the normalized values of the average annual growing season representing NDVI, EVI, and SIF, SMsurf, SMroot, SPEI07 (the cumulative 7-month water deficit event), temperature, precipitation, and net solar radiation, respectively; the dashed lines are the relative fit lines, and the shaded area indicates the standard deviation.

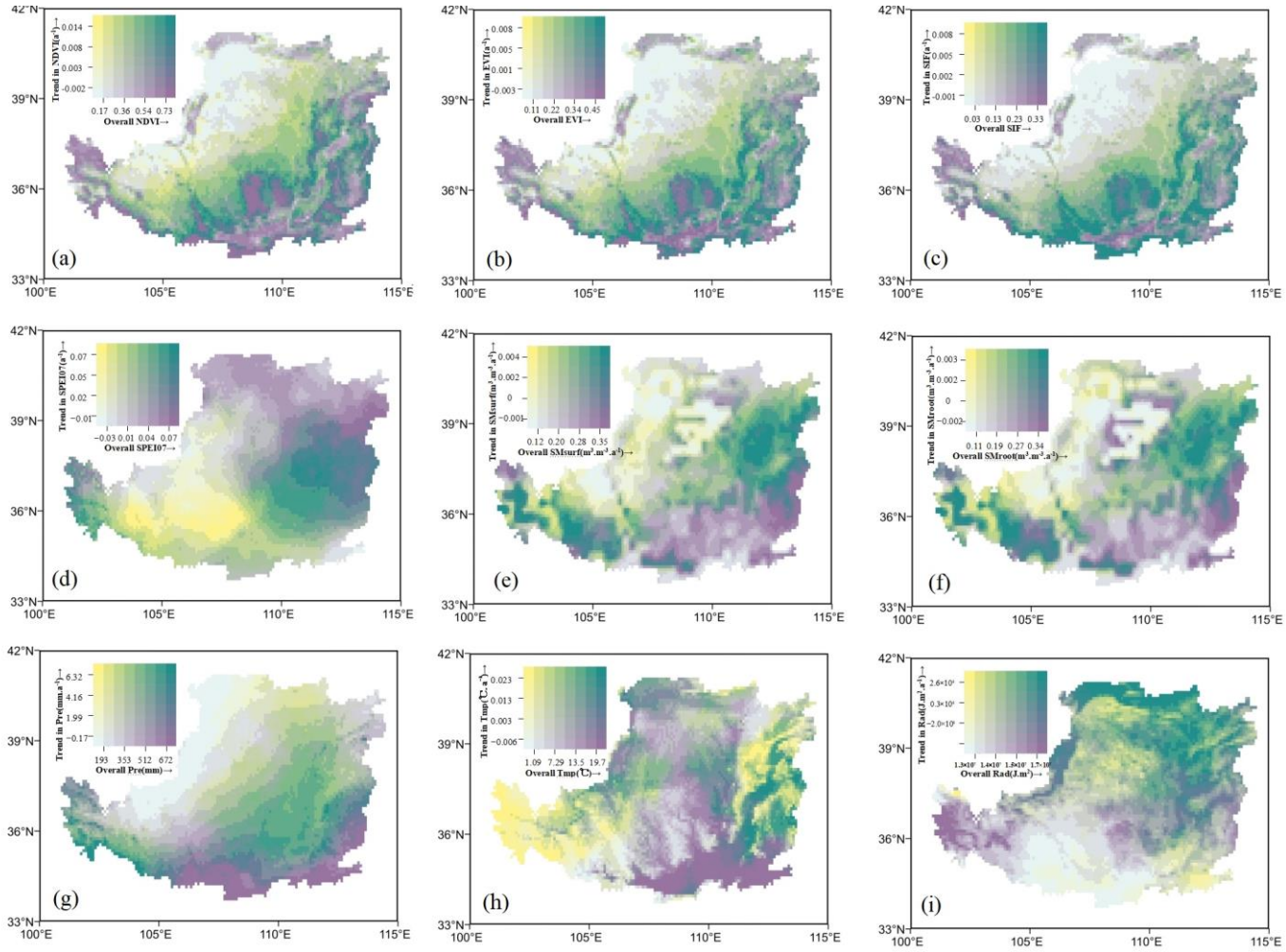

Figure 6. Bivariate map of annual mean and slope of vegetation growth indices, water availability indices and meteorological indices. (**a**–**c**) indicate NDVI, EVI, and SIF, respectively; (**d**–**f**) indicate SMsurf, SMroot, SPEI07 (7-month cumulative water balance), respectively; (**g**–**i**) indicate precipitation, temperature and net solar radiation, respectively.

Meteorological drought conditions in the Loess Plateau changed from wet in the northeast to arid in the southwest, as depicted in Figure 6. The annual average growing season SPEI07 displayed a decreasing trend of 6.18%, primarily in the northern part. However, this does not necessarily indicate a risk of drought or vegetation water stress, since SPEI is a meteorological water resource effectiveness indicator that compares wet to dry conditions in an area to the long-term average, with high to low values [19]. The Hurst index of the annual average SPEI07 ranged from 0.24 to 0.45, indicating an overall inverse persistence of water deficit in the cumulative 7 months of the annual average growing season. The multi-year average growing season of SPEI07 showed a gradual increase in the moisture conditions in the semi-humid climate zone, semi-arid climate zone, and arid climate zone, with the semi-humid climate zone exhibiting the largest rate of increase in moisture. Only 11% of the areas exhibited significantly wetter meteorology, primarily distributed in the semi-humid climate zone. When examining the SPEI07 of the multi-year average growing season, the moisture conditions in the semi-arid climate zone were found to be better than those in the semi-humid and arid climate zones, since the SPEI calculation not only considers precipitation conditions, but also integrates the influence of temperature.

3.2. Response Characteristics of Vegetation to Water Deficit

3.2.1. The Most Sensitive Time Scale of Vegetation to Water Deficit

The timescale at which vegetation was most affected by the water deficit, determined by the timescale corresponding to the maximum positive correlation coefficient (Figure 7a,b), was used to analyze the relationship between vegetation growth and water deficit in the Loess Plateau from 2000 to 2020. The results showed that the average response time was 6.43 months, with 7.53 months in the arid climate zone, 6.28 months in the semi-arid climate zone, and 6.19 months in the semi-humid climate zone. Vegetation growth was the most impacted by water deficit events lasting 6–8 months, making 7 months the reasonable timescale to investigate the moisture deficit of vegetation. Regions with a response time greater than 7 months were mainly located in the northwestern section, with a few in the north and south-southeast. For the multi-year average growing season, the decreasing and increasing trends in response time accounted for 37.15% and 26.84% of the region's total area, respectively. An increasing response time indicated that the vegetation in the region was more drought-resistant and less sensitive to drought, while a decreasing response time indicated the opposite, requiring that attention be paid to the adverse effects of water deficit on vegetation growth. The characteristics of the response of vegetation to drought showed apparent spatial and temporal heterogeneity. The areas where the response time decreased were mainly in the northern part of the Loess Plateau, mostly in the semi-arid climate zone, while the areas where the response time increased were mainly distributed in the southwestern part of the arid climate zone and semi-arid climate zone, as well as the southeastern part of the semi-humid region.

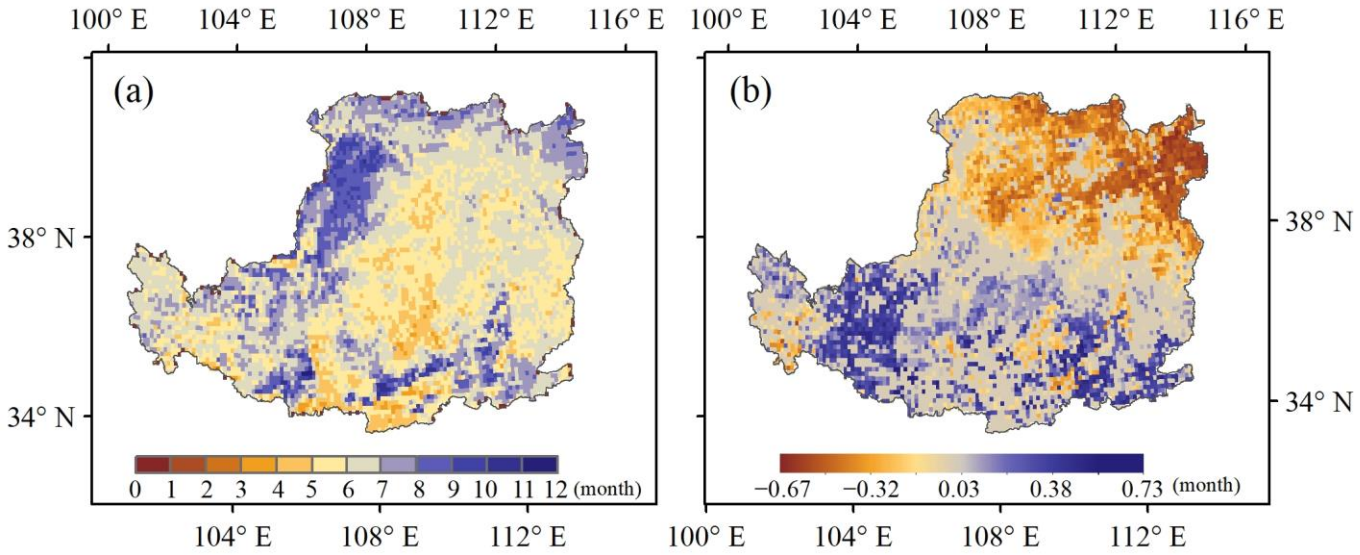

Figure 7. Multi-year average (**a**) and slope (**b**) of the response time of vegetation growth to water deficit.

3.2.2. The Timescale Showing the Most Sensitive of Periods of Vegetation at Different Growth Stages to Water Deficit

To examine the impact of water availability on vegetation during different stages of growth, this study divided the growing season into three sub-stages: the early growing season (April–June), the mid growing season (June–August), and the late growing season (August–October). The value of the maximum correlation coefficient between NDVI and SPEI (Rmax) indicated the extent to which vegetation growth was affected by water deficit and the duration of the vegetation growth response to water surplus and deficit. On average, the Rmax value for the entire growing season is 0.38, with values of 0.26, 0.35, and 0.29 for April–June, June–August, and August-October, respectively, highlighting that vegetation growth is the most impacted by water deficit in the mid growing season. The maximum response of the semi-humid and arid climate zones to water deficit was not

significantly different, and the response for both of these areas was higher than that in the semi-arid climate zone. June to August show the highest vegetation response to water deficit. The average response scale of vegetation growth to water deficit in the growing season was 7.8 months, with an average response timescale of 9 months in April–June, 5.7 months in June–August, and 6.5 months in August–October. Therefore, vegetation growth was found to be the most sensitive to water deficit in June-August, indicating the need to pay close attention to the impact of water deficit on vegetation growth during this period.

3.2.3. Response of Different Vegetation Types to Water Deficit

The dominant vegetation types in the study area are mainly cultivated vegetation and grasses, which accounted for 45.03% and 32.96% of the total vegetation coverage, respectively. Shrubs, broadleaved forests, coniferous forests, and alpine vegetation accounted for 7.71%, 5.43%, 3.09%, and 0.07%, respectively. Cultivated vegetation is mainly grown in the semi-arid and semi-humid climate zones, accounting for 61.81% and 32.54% of the total cultivated area, respectively. Grasses are predominantly distributed in the semi-arid climate zone and the arid climate zone, accounting for 76.28% and 16.74% of the total cultivated area, respectively.

As depicted in Figure 8, the degree of response and the timescale of vegetation growth in response to the water deficit varied across different growth stages and vegetation types. In the growing season, grasses were the most affected by the water deficit, followed by cultivated forests and shrubs, while alpine vegetation showed the least sensitivity to the water deficit. During the late growing season (August to October), grasses and cultivated forests were the plants most affected by the water deficit, whereas coniferous forests and broadleaved forests, as well as alpine forests, showed maximum sensitivity in the mid growing season (June to August). Moreover, the response time of VWD during the growing season also varied among different vegetation types, with grasses exhibiting the highest response time, followed by alpine forests, shrubs, cultivated forests, broadleaved forests, and coniferous forests. Although grasses were the least sensitive vegetation regarding the response time to water deficit during the growing season (Figure 8), their sensitivity varied across different growing seasons. In the early growing season, broadleaved forests were the most sensitive vegetation to water deficit, while grasses were the least sensitive. In the middle of the growing season, alpine forests showed the least sensitivity to water deficit, while grasses were the most sensitive. During the late growing season, grasses remained the vegetation most sensitive to water deficit, while coniferous forests were the least sensitive. These differences in vegetation water requirements, timescales, and critical growth periods should be considered when assessing the impact of water deficit on vegetation [3,5]. The response characteristics and sensitivity of different vegetation types to water availability vary, leading to spatial and temporal heterogeneity in the response of vegetation growth to water availability.

3.3. Sustainable Development of Vegetation Growth in the Loess Plateau

3.3.1. Determining the Future Growth of Vegetation

The sustainability of future changes in vegetation and meteorological drought was determined by trend analysis and Hurst index calculations. Figure 9 shows that 93.90% of the Loess Plateau exhibited improved and weakly reversed changes (improvement and anti-sustainability) in moisture condition, with 0.02% classified as strong anti-sustainability, 58.57% as medium anti-sustainability, and 35.32% as weak anti-sustainability. However, 6.10% of the area is expected to transition from dry to wet. Although the majority of the area is expected to become wetter, the potential for anti-sustainable changes should be addressed. Between 2000 and 2020, vegetation restoration improved in 98.59% of the total area of the Loess Plateau, with 59.24% experiencing improvement, but with weak anti-sustainability, and 28.70% experiencing weak persistence. Therefore, the future trend of vegetation restoration requires attention, particularly in improved and anti-sustainable areas. Analyzing the

causes of vegetation restoration and improving the external environment of vegetation growth is crucial for forestry development and scientific management. Vigilance and concern for the health of vegetation restoration are necessary to ensure sustainability.

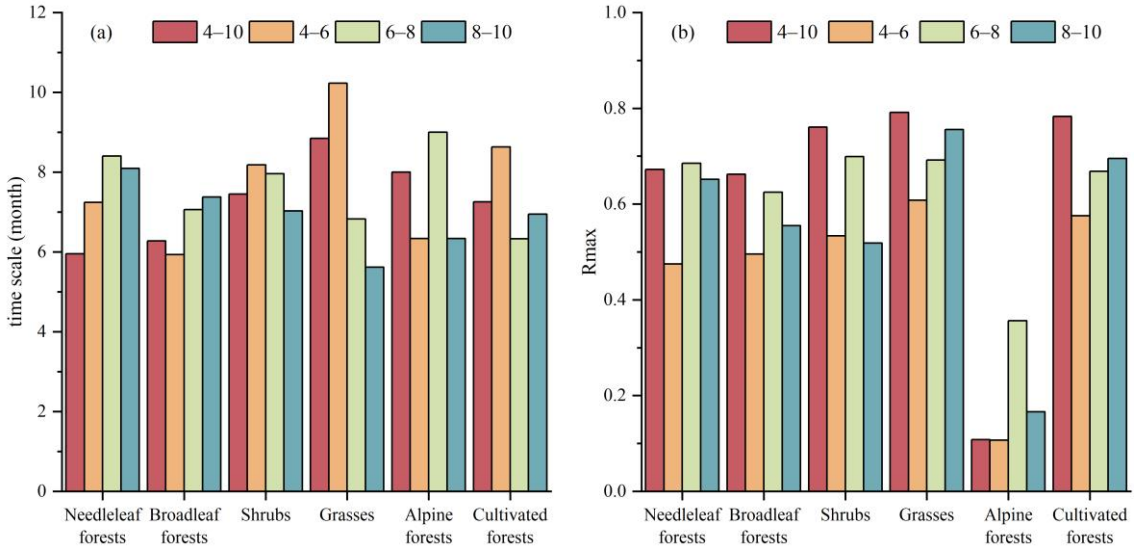

Figure 8. Time scales (**a**) and Rmax (**b**) for the response of various vegetation species to water surplus and deficit.

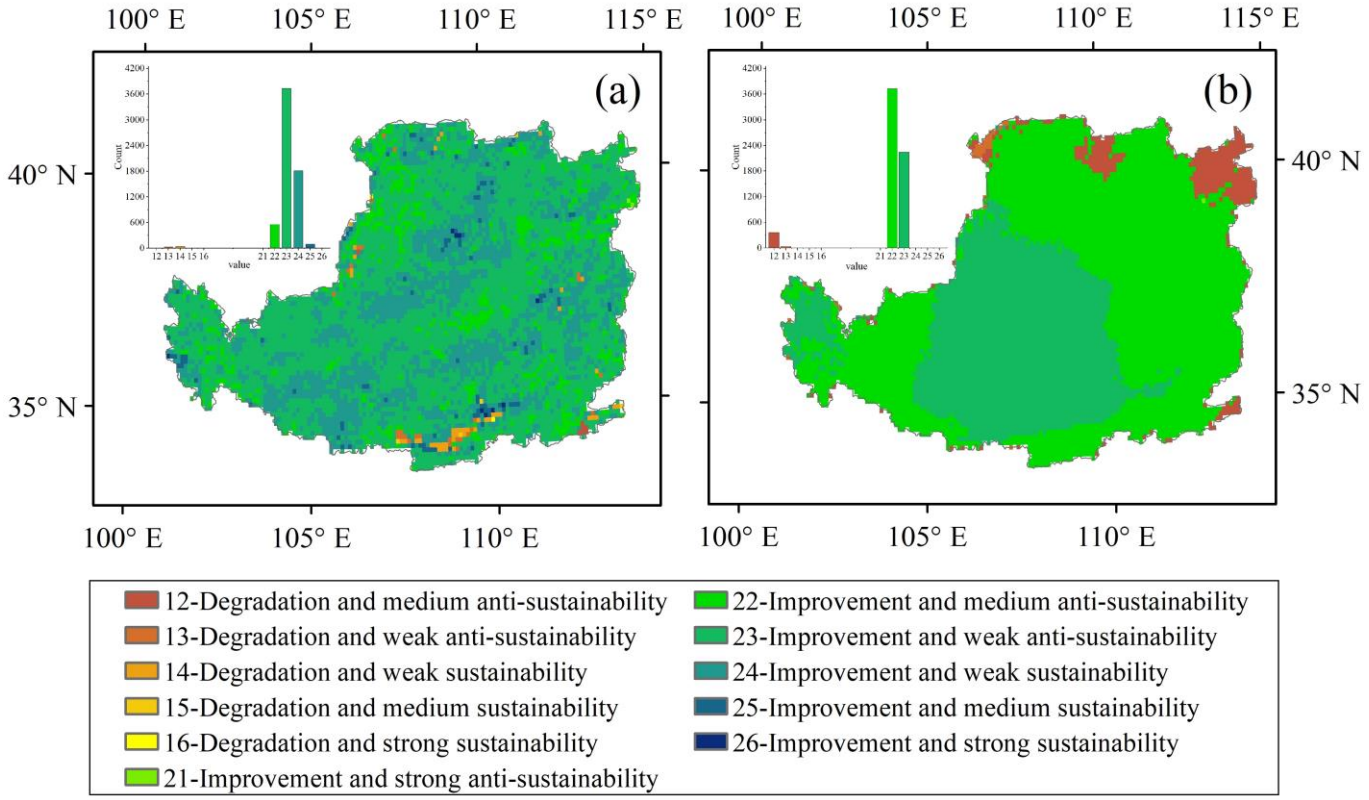

Figure 9. Sustainability of vegetation growth and changes in moisture conditions during the growing season in the Loess Plateau. (**a**,**b**) represent the trend and sustainability of NDVI and SPEI07, respectively.

3.3.2. Dominant Environmental Factors of Vegetation Growth

The restoration of vegetation is mainly influenced by human beings, especially regarding the conversion of farmland to forests and grasses. However, environmental factors, such as temperature, precipitation, soil moisture, and solar radiation, also play a crucial role in vegetation growth [56]. To identify the relatively more important factors, standardized regression coefficients were used. As illustrated in Figure 10, temperature, precipitation, root-zone soil moisture, and solar radiation accounted for 2.78%, 27.48%, 51.56%, and 18.18% of vegetation growth, respectively. Soil moisture was the dominant factor in most areas, followed by precipitation. However, the dominant factor of vegetation growth varies by climatic zones. In the arid and semi-arid climate zones, soil moisture is the most critical factor, while solar radiation is the dominant factor in the semi-humid climate zones. The effect of soil moisture on vegetation growth is more direct than that of precipitation, especially in areas where vegetation growth is limited by moisture, such as arid and semi-arid regions [57,58]. Furthermore, the response of vegetation to environmental factors such as temperature and precipitation differs among regions due to differences in hydrothermal conditions and vegetation types [59,60]. Each climate zone has a unique ecosystem structure, and different ecosystems have varying water use efficiencies [61], resulting in different sensitivities to water surplus and deficit [17] and different response characteristics in each climate zone [13]. Hence, understanding the impacts of environmental factors on vegetation growth is crucial for scientific management and sustainable forestry development.

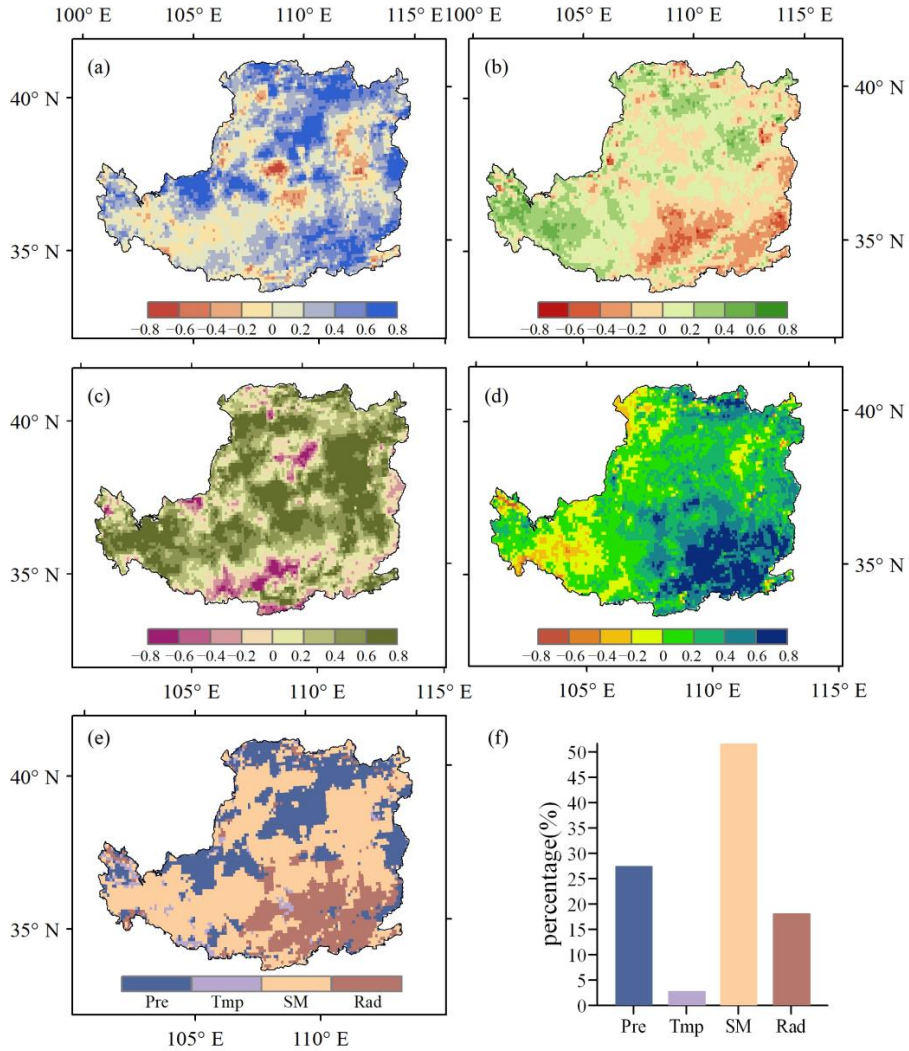

Figure 10. Spatial distribution of dominant environmental factors for vegetation growth. (**a**–**d**) represent the standardized regression coefficients of precipitation, temperature, root-zone soil moisture,

and net solar radiation, respectively; (**e**,**f**) represent the dominant environmental factors for vegetation growth (Pre = precipitation, Tmp = temperature, SM = root-zone soil moisture, and Rad = net solar radiation).

4. Discussion

4.1. Response of Vegetation to Water Surplus and Deficit in Different Climatic Zones

The Loess Plateau is experiencing changes in VWD and vegetation water surplus, with the VWD area contracting and the vegetation water surplus area expanding. This indicates that vegetation growth is hindered by a weakening water deficit and an increase in vegetation water surplus due to the improved humidity conditions. The vegetation water surplus area is relatively small and mainly located in the subhumid climate area on the southern margin of the Loess Plateau, which is prone to rain and flooding during the flood season occurring in different years [62]. The occurrence of rain-caused flooding, especially heavy flooding, negatively affects vegetation or crops with low water demand, resulting in excess vegetation water in a few areas in the southern Loess Plateau. The changes in the VWD area vary among different climate zones, with the arid and semi-humid climate zones showing a trend of contraction, while the semi-arid climate zone exhibits a non-significant increase and a trend of VWD area expansion. The semi-arid climate zone is rich in vegetation types, with cultivated vegetation and grasses being the two vegetation types most affected by drought. In recent years, the implementation of the project of returning farmland to forests and grasses has resulted in the addition of many new areas of cultivated vegetation and grasses in the Loess Plateau, but the water-consuming effect of planted forests is significantly greater than their water-holding effect, leading to widespread dry soil layers in the Loess area [63]. Therefore, the expansion trend of VWD areas in the semi-arid climate zone may be attributed to plantation forestry and grasses, which is yet to be proved by future investigation.

4.2. Response Characteristics of Vegetation Growth to Water Deficit Events in the Loess Plateau at Multiple Timescales

Vegetation growth responds heterogeneously to drought at multiple spatial and temporal scales. The response time of vegetation to water deficit events varies among different climate zones, with the arid climate zone showing the longest average response time, followed by the semi-arid climate zone. This variability can be attributed to the varying sensitivity, resistance, and resilience of biomes to cumulative water deficit events in different climate zones. Plants in arid regions may have developed mechanisms to rapidly adapt to a changing water supply, which could explain their rapid response to below-normal water conditions. Conversely, plants in semi-arid and semi-humid biomes have different physiological mechanisms that are less adapted to water scarcity and can only tolerate it to a limited extent. However, their response rate to drought is slower than that of arid biomes. Therefore, the average response time of semi-arid and dry-humid zones is shorter than that of arid zones [8]. Control indicators that affect the response of vegetation growth to the water supply include, but are not limited to, soil moisture, soil properties, surface temperature, snow cover area, land use types, and intensity of human activities [36,64–67]. Therefore, an exploration of the dominant factors regarding the spatial heterogeneity of the response characteristics of vegetation growth to water availability, which is essential to improve the accuracy of vegetation change prediction, should be considered in the future.

4.3. Uncertainty

The study utilized NDVI and SPEI at different timescales to determine and examine the expansion or contraction trend of the VWD and vegetation surplus in the Loess Plateau. Additionally, it analyzed the response characteristics and sensitivity changes of vegetation to SPEI at different timescales. The Thornthwaite method was used to calculate PET (potential evapotranspiration). The calculation accuracy of PET will affect the calculation results of SPEI; thus, it is an uncertain point. Regarding the analysis, the period of the study

was restricted to only 21 years due to the limitations of time and the resolution of the data, so the sliding window of 5 years was employed for calculation and analysis. this period is insufficient for verifying the robustness of the sliding window analysis results over larger sliding window periods, such as 10 years and 15 years, nor is it long enough to analyze the periodic changes of VWD. In future studies, the research timescale can be extended, and the data resolution can be improved using multi-source remote sensing data. Moreover, multiple analysis windows of different sizes can be studied to validate one another and to generate more robust findings.

5. Conclusions

In order to investigate the response of vegetation to water deficit under climate change conditions, as well as and its response mechanism, the general trend of VWD and the changes in different climatic zones were analyzed. It was found that the overall trend of the VWD area exhibited a non-significant increase, which was caused by the varying changes in different climatic zones. Specifically, the arid and semi-humid climatic zones showed a trend of contraction, while the semi-arid climatic zone showed a trend of non-significant expansion. Although the expansion trend of the VWD area may seem insignificant in the view of the semi-arid climate zone, it poses a potential danger and cannot be ignored. To understand why the VWD area in the semi-arid climate area was not significantly expanded, the study examined the response time and sensitivity of vegetation to water deficit, the response time of vegetation at different growth stages, and the response time of different vegetation types. The findings revealed that vegetation growth is most significant in the semi-arid climate area, with grasses and cultivated vegetation being the primary types. These factors could be the reason for the potential threat of water shortage for vegetation in the semi-arid climate area. The study results can provide some scientific recommendations, such as choosing vegetation types that are less sensitive to drought in these zones or focusing on studying the effects of drought on vegetation during the mid of the growing season, for vegetation research and management in arid and semi-arid climatic zones.

Supplementary Materials: The following supporting information can be downloaded at: https://www.mdpi.com/article/10.3390/rs15102593/s1, Figure S1: Correlation of the drought index results calculated in this study with SPEIbase v2.5; Figure S2: Comparison of the time trends between the drought index results calculated in this paper and SPEIbase v2.5; Table S1: Vegetation cover type re-classification.

Author Contributions: Conceptualization, Y.L., W.L. and J.Y.; methodology, Y.L.; software, Y.L.; validation, Y.L.; formal analysis, Y.L. and J.Y.; investigation, Y.L.; resources, Y.L.; data curation, Y.L.; writing—original draft preparation, Y.L. and J.Y.; writing—review and editing, Y.L., W.L., J.Y., W.Z., F.G., C.W. and X.L.; visualization, Y.L.; supervision, W.L., J.Y., W.Z., F.G., C.W. and X.L.; project administration, W.L. and J.Y.; funding acquisition, W.L. and J.Y. All authors have read and agreed to the published version of the manuscript.

Funding: This work was conducted with financial support from the Natural Science Basic Research Plan of Shaanxi Province (2023-JC-YB-275), the National Natural Science Foundation of China (42071144), the Fundamental Research Funds for the Central Universities, Shaanxi Normal University (2021CBWY003) and Special Scientific Research Project of Shaanxi Normal University (22YDYLZ002).

Data Availability Statement: The monthly temperature and precipitation data are available from the National Science and Technology Infrastructure Platform-National Earth System Science Data Center. The temperature data is available at http://www.geodata.cn/data/datadetails.html?dataguid=164304785536614&docId=1839, accessed on 17 May 2022, while the precipitation data is available at http://www.geodata.cn/data/datadetails.html?dataguid=192891852410344&docid=1165, accessed on 11 May 2022. The GLEAM soil moisture data can be obtained from https://www.GLEAM.eu, accessed on 18 October 2021. The moderate resolution imaging spectroradiometer (MOD13C2, V6)-based NDVI and EVI datasets are available at https://ladsweb.modaps.eosdis.nasa.gov/, accessed on 5 May 2022. Monthly GOSIF data were obtained from http://data.globalecology.unh.edu/data/

GOSIF_v2/Monthly/, accessed on 7 June 2022. Vegetation cover type data were provided by the Data Center for Resources and Environmental Sciences of Chinese Academy of Sciences, available at https://www.resdc.cn/data.aspx?DATAID=122, accessed on 1 October 2022. The net surface solar radiation can be obtained from https://cds.climate.copernicus.eu/cdsapp#!/dataset/reanalysis-era5-land-monthly-means?tab=overview, accessed on 18 May 2022.

Acknowledgments: The authors acknowledge the funding sponsors listed above. The authors also acknowledge the National Earth System Science Data Center, National Science and Technology Infrastructure of China. (http://www.geodata.cn, accessed on 11 May 2022) for data support.

Conflicts of Interest: The authors declare no conflict of interest.

References

1. Diffenbaugh, N.S.; Pal, J.S.; Trapp, R.J.; Giorgi, F. Fine-scale processes regulate the response of extreme events to global climate change. *Proc. Natl. Acad. Sci. USA* **2005**, *102*, 15774–15778. [CrossRef] [PubMed]
2. Dai, A. Drought under global warming: A review. *WIREs Clim. Chang.* **2010**, *2*, 45–65. [CrossRef]
3. Qi, G.; Song, J.; Li, Q.; Bai, H.; Sun, H.; Zhang, S.; Cheng, D. Response of vegetation to multi-timescales drought in the Qinling Mountains of China. *Ecol. Indic.* **2022**, *135*, 108539. [CrossRef]
4. Ivits, E.; Horion, S.; Fensholt, R.; Cherlet, M. Drought footprint on European ecosystems between 1999 and 2010 assessed by remotely sensed vegetation phenology and productivity. *Glob. Chang. Biol.* **2014**, *20*, 581–593. [CrossRef] [PubMed]
5. Zhang, Q.; Kong, D.; Singh, V.P.; Shi, P. Response of vegetation to different time-scales drought across China: Spatiotemporal patterns, causes and implications. *Glob. Planet. Chang.* **2017**, *152*, 1–11. [CrossRef]
6. Peterson, T.J.; Saft, M.; Peel, M.C.; John, A. Watersheds may not recover from drought. *Science* **2021**, *372*, 5. [CrossRef]
7. Berdugo, M.; Delgado-Baquerizo, M.; Soliveres, S.; Hernández-Clemente, R.; Zhao, Y.; Gaitán, J.J.; Gross, N.; Saiz, H.; Maire, V.; Lehmann, A.; et al. Global ecosystem thresholds driven by aridity. *Science* **2020**, *367*, 787–790. [CrossRef]
8. Vicente-Serrano, S.M.; Gouveia, C.; Camarero, J.J.; Begueria, S.; Trigo, R.; Lopez-Moreno, J.I.; Azorin-Molina, C.; Pasho, E.; Lorenzo-Lacruz, J.; Revuelto, J.; et al. Response of vegetation to drought time-scales across global land biomes. *Proc. Natl. Acad. Sci. USA* **2013**, *110*, 52–57. [CrossRef]
9. Qian, X. Construction of Vegetation Drought Stress Index Based on Solar-Induced Chlorophyll Fluorescence. Master's Thesis, Nanjing University, Nanjing, China, 2019.
10. Du, P.; Arndt, S.K.; Farrell, C. Is plant survival on green roofs related to their drought response, water use or climate of origin? *Sci. Total Environ.* **2019**, *667*, 25–32. [CrossRef]
11. Anderegg, W.R.L.; Schwalm, C.; Biondi, F.; Camarero, J.J.; Koch, G.; Litvak, M.; Ogle, K.; Shaw, J.D.; Shevliakova, E.; Williams, A.P.; et al. Pervasive drought legacies in forest ecosystems and their implications for carbon cycle models. *Science* **2015**, *349*, 528–532. [CrossRef]
12. Zhang, X.Y.; Zhang, B.Q. The responses of natural vegetation dynamics to drought during the growing season across China. *J. Hydrol.* **2019**, *574*, 706–714. [CrossRef]
13. Zhao, A.; Zhang, A.; Cao, S.; Liu, X.; Liu, J.; Cheng, D. Responses of vegetation productivity to multi-scale drought in Loess Plateau, China. *Catena* **2018**, *163*, 165–171. [CrossRef]
14. Pasho, E.; Camarero, J.J.; de Luis, M.; Vicente-Serrano, S.M. Impacts of drought at different time scales on forest growth across a wide climatic gradient in north-eastern Spain. *Agric. For. Meteorol.* **2011**, *151*, 1800–1811. [CrossRef]
15. McDowell, N.; Pockman, W.T.; Allen, C.D.; Breshears, D.D.; Cobb, N.; Kolb, T.; Plaut, J.; Sperry, J.; West, A.; Williams, D.G.; et al. Mechanisms of plant survival and mortality during drought: Why do some plants survive while others succumb to drought? *New Phytol.* **2008**, *178*, 719–739. [CrossRef]
16. Zhou, J.; Jia, L.; Menenti, M.; van Hoek, M.; Lu, J.; Zheng, C.; Wu, H.; Yuan, X. Characterizing vegetation response to rainfall at multiple temporal scales in the Sahel-Sudano-Guinean region using transfer function analysis. *Remote Sens. Environ.* **2021**, *252*, 112108. [CrossRef]
17. Ding, Y.; Xu, J.; Wang, X.; Peng, X.; Cai, H. Spatial and temporal effects of drought on Chinese vegetation under different coverage levels. *Sci. Total Environ.* **2020**, *716*, 137166. [CrossRef]
18. Ciais, P.; Reichstein, M.; Viovy, N.; Granier, A.; Ogee, J.; Allard, V.; Aubinet, M.; Buchmann, N.; Bernhofer, C.; Carrara, A.; et al. Europe-wide reduction in primary productivity caused by the heat and drought in 2003. *Nature* **2005**, *437*, 529–533. [CrossRef]
19. Vicente-Serrano, S.M.; Begueria, S.; Lopez-Moreno, J.I. A Multiscalar Drought Index Sensitive to Global Warming: The Standardized Precipitation Evapotranspiration Index. *J. Clim.* **2010**, *23*, 1696–1718. [CrossRef]
20. Mishra, A.K.; Singh, V.P. A review of drought concepts. *J. Hydrol.* **2010**, *391*, 202–216. [CrossRef]
21. Willmott, C.J.; Feddema, J.J. A more rational climatic moisture index. *Prof. Geogr.* **1992**, *44*, 84–88. [CrossRef]
22. Guttman, N.B. Accepting the standardized precipitation index:a calculation algorithm. *J. Am. Water Resour. Assoc.* **1999**, *35*, 311–322. [CrossRef]
23. Mckee, T.B.; Doesken, N.J.; Kleist, J. The relationship of drought frequency and duration to time scales. In Proceedings of the 8th Conference on Applied Climatology, Anaheim, CA, USA, 17–22 January 1993; pp. 179–186.

24. West, H.; Quinn, N.; Horswell, M. Remote sensing for drought monitoring & impact assessment: Progress, past challenges and future opportunities. *Remote Sens. Environ.* **2019**, *232*, 111291. [CrossRef]
25. Wang, Y.; Fu, B.; Liu, Y.; Li, Y.; Feng, X.; Wang, S. Response of vegetation to drought in the Tibetan Plateau: Elevation differentiation and the dominant factors. *Agric. For. Meteorol.* **2021**, *306*, 108468. [CrossRef]
26. Li, C.; Leal Filho, W.; Yin, J.; Hu, R.; Wang, J.; Yang, C.; Yin, S.; Bao, Y.; Ayal, D.Y. Assessing vegetation response to multi-time-scale drought across inner Mongolia plateau. *J. Clean. Prod.* **2018**, *179*, 210–216. [CrossRef]
27. Li, M.; Ge, C.; Zong, S.; Wang, G. Drought Assessment on Vegetation in the Loess Plateau Using a Phenology-Based Vegetation Condition Index. *Remote Sens.* **2022**, *14*, 3043. [CrossRef]
28. Li, X.Y.; Duan, Z.H. Review on the Interaction between Soil Moisture and Vegetation on the Loess Plateau. *J. Soil Sci.* **2012**, *43*, 1508–1514. [CrossRef]
29. He, B.; Huang, L.; Chen, Z.; Wang, H. Weakening sensitivity of global vegetation to long-term droughts. *Sci. China Earth Sci.* **2017**, *61*, 60–70. [CrossRef]
30. Zhang, Y.W.; Wan, S.S.; Wang, J. Soil Water Deficit During Vegetation Succession on the Loess Plateau. *Res. Soil Water Conserv.* **2020**, *27*, 120–125. [CrossRef]
31. Fan, Q.; Zhao, A.Z.; Wang, J. Spatiotemporal evolution of NDVI and its seasonal response to climate change in the Loess Plateau from 1982 to 2015. *Chin. J. Ecol.* **2020**, *39*, 1664–1675. [CrossRef]
32. Wang, Y.R.; Wang, X.W. Analyses on Spatial-Temporal Change Characteristics of Rainfall over Chinese Loess Plateau from April to October. *Plateau Meteorol.* **2006**, *25*, 737–743.
33. Xie, B.; Jia, X.; Qin, Z.; Shen, J.; Chang, Q. Vegetation dynamics and climate change on the Loess Plateau, China: 1982–2011. *Reg. Environ. Chang.* **2015**, *16*, 1583–1594. [CrossRef]
34. Peng, S.; Ding, Y.; Liu, W.; Li, Z. 1 km monthly temperature and precipitation dataset for China from 1901 to 2017. *Earth Syst. Sci. Data* **2019**, *11*, 1931–1946. [CrossRef]
35. Ji, L.; Peters, A.J. Assessing vegetation response to drought in the northern Great Plains using vegetation and drought indices. *Remote Sens. Environ.* **2003**, *87*, 85–98. [CrossRef]
36. Niu, Y.; Yang, S.; Zhou, J.; Chu, B.; Ma, S.; Zhu, H.; Hua, L. Vegetation distribution along mountain environmental gradient predicts shifts in plant community response to climate change in alpine meadow on the Tibetan Plateau. *Sci. Total Environ.* **2019**, *650*, 505–514. [CrossRef]
37. Martens, B.; Miralles, D.G.; Lievens, H.; Schalie, R.V.D.; Richard, A.M.d.J.; Fernandez-Prieto, D.; Beck, H.E.; Dorigo, W.A.; Verhoest, N.E.C. GLEAM v3: Satellite-based land evaporation and root-zone soil moisture. *Geosci. Model Dev. Discuss.* **2016**, *10*, 1903–1925. [CrossRef]
38. Miralles, D.G.; Holmes, T.R.H.; De Jeu, R.A.M.; Gash, J.H.; Meesters, A.G.C.A.; Dolman, A.J. Global land-surface evaporation estimated from satellite-based observations. *Hydrol. Earth Syst. Sci.* **2011**, *15*, 453–469. [CrossRef]
39. Ye, L.; Fang, L.; Shi, Z.; Deng, L.; Tan, W. Spatio-temporal dynamics of soil moisture driven by 'Grain for Green' program on the Loess Plateau, China. *Agric. Ecosyst. Environ.* **2019**, *269*, 204–214. [CrossRef]
40. Wang, X.G.; Lu, X.T.; Zhang, H.Y.; Dijkstra, F.A.; Jiang, Y.-G.; Wang, X.-B.; Lu, J.Y.; Wu, Y.N.; Wang, Z.W.; Han, X.G. Changes in soil C:N:P stoichiometry along an aridity gradient in drylands of northern China. *Geoderma* **2020**, *361*, 114087. [CrossRef]
41. Li, J.; Chen, F.; Zhang, G.; Barlage, M.; Gan, Y.; Xin, Y.; Wang, C. Impacts of Land Cover and Soil Texture Uncertainty on Land Model Simulations Over the Central Tibetan Plateau. *J. Adv. Model. Earth Syst.* **2018**, *10*, 2121–2146. [CrossRef]
42. Bronick, C.J.; Lal, R. Soil structure and management: A review. *Geoderma* **2005**, *124*, 3–22. [CrossRef]
43. Grace, J.; Nichol, C.; Disney, M.; Lewis, P.; Quaife, T.; Bowyer, P. Can we measure terrestrial photosynthesis from space directly, using spectral reflectance and fluorescence? *Glob. Chang. Biol.* **2007**, *13*, 1484–1497. [CrossRef]
44. Gamon, J.A.; Field, C.B.; Goulden, M.L.; Griffin, K.L.; Hartley, A.E.; Josep Penuelas, G.J.; Valentini, R. Relationships between NDVI, canopy structure, and photosynthesis in three Californian vegetation types. *Ecol. Appl.* **1995**, *5*, 28–41. [CrossRef]
45. Zhou, L.; Tian, Y.; Myneni, R.B.; Ciais, P.; Saatchi, S.; Liu, Y.Y.; Piao, S.; Chen, H.; Vermote, E.F.; Song, C.; et al. Widespread decline of Congo rainforest greenness in the past decade. *Nature* **2014**, *509*, 86–90. [CrossRef] [PubMed]
46. Guanter, L.; Zhang, Y.; Jung, M.; Joiner, J.; Voigt, M.; Berry, J.A.; Frankenberg, C.; Huete, A.R.; Zarco-Tejada, P.; Lee, J.E.; et al. Global and time-resolved monitoring of crop photosynthesis with chlorophyll fluorescence. *Proc. Natl. Acad. Sci. USA* **2014**, *111*, E1327–E1333. [CrossRef]
47. Mohammed, G.H.; Colombo, R.; Middleton, E.M.; Rascher, U.; van der Tol, C.; Nedbal, L.; Goulas, Y.; Perez-Priego, O.; Damm, A.; Meroni, M.; et al. Remote sensing of solar-induced chlorophyll fluorescence (SIF) in vegetation: 50 years of progress. *Remote Sens. Environ.* **2019**, *231*, 111177. [CrossRef]
48. Li, X.; Xiao, J. A Global, 0.05-Degree Product of Solar-Induced Chlorophyll Fluorescence Derived from OCO-2, MODIS, and Reanalysis Data. *Remote Sens.* **2019**, *11*, 517. [CrossRef]
49. Kong, D.; Zhang, Q.; Gu, X.H. Vegetation responses to drought at different time scales in China. *Acta Ecol. Sin.* **2016**, *36*, 7908–7918.
50. Jiao, W.; Wang, L.; Smith, W.K.; Chang, Q.; Wang, H.; D'Odorico, P. Observed increasing water constraint on vegetation growth over the last three decades. *Nat. Commun.* **2021**, *12*, 3777. [CrossRef]
51. Zhang, Q.; Tang, H.P.; Cui, F.Q. SPEI-based analysis of drought characteristics and trends in Hulun Buir grassland. *Acta Ecol. Sin.* **2019**, *39*, 7110–7123.

52. Tang, B.Q.; Yan, J.P.; Cao, Y.W. The response of extreme temperature events to climate warming in Fujian Province. *J. China Agric. Univ.* **2016**, *21*, 123–132.
53. Wang, B.; Xu, G.; Li, P.; Li, Z.; Zhang, Y.; Cheng, Y.; Jia, L.; Zhang, J. Vegetation dynamics and their relationships with climatic factors in the Qinling Mountains of China. *Ecol. Indic.* **2020**, *108*, 105719. [CrossRef]
54. Deng, R.L.; Yang, Y.k.; Li, Q. Applicability and drought evolution analysis of drought index in Zhangye City. *China Rural Water Hydropower* **2021**, 106–113.
55. Zhuang, S.W.; Zuo, H.C.; Ren, H.C. Application of standardized precipitation evapotranspiration index in China. *Clim. Environ. Res. (Chin.)* **2013**, *18*, 617–625.
56. Yang, L.; Liu, L.N.; Sun, S.B. The dominated environmental factors of vegetation change on the Qinghai-Tibet Plateau from 1982 to 2015. *Acta Ecol. Sin.* **2021**, *43*, 744–755.
57. Coners, F.; Babel, W.; Willinghofer, S.; Biermann, T.; Kohler, L.; Seeber, E.; Foken, T.; Ma, Y.M.; Yang, Y.P.; Miehe, G.; et al. Evapotranspiration and water balance of high-elevation grassland on the Tibetan Plateau. *J. Hydrol.* **2016**, *533*, 557–566. [CrossRef]
58. Li, G.; Sun, S.; Han, J.; Yan, J.; Liu, W.; Wei, Y.; Lu, N.; Sun, Y. Impacts of Chinese Grain for Green program and climate change on vegetation in the Loess Plateau during 1982–2015. *Sci. Total Environ.* **2019**, *660*, 177–187. [CrossRef]
59. Zhong, L.; Ma, Y.; Xue, Y.; Piao, S. Climate Change Trends and Impacts on Vegetation Greening Over the Tibetan Plateau. *J. Geophys. Res.-Atmos.* **2019**, *124*, 7540–7552. [CrossRef]
60. Li, H.Y.; Zhang, C.G.; Wang, S.Z. Response of vegetation dynamics to hydrothermal conditions on the Qinghai-Tibet Plateau in the last 40 years. *Acta Ecol. Sin.* **2022**, *42*, 4770–4783.
61. Yang, Y.; Guan, H.; Batelaan, O.; McVicar, T.R.; Long, D.; Piao, S.; Liang, W.; Liu, B.; Jin, Z.; Simmons, C.T. Contrasting responses of water use efficiency to drought across global terrestrial ecosystems. *Sci. Rep.* **2016**, *6*, 23284. [CrossRef]
62. Wu, G.; Fu, S.H.; Yin, B. Spatial and temporal distribution of drought and flood in Loess Plateau in different hydrological years. *Agric. Eng.* **2022**, *12*, 65–71. [CrossRef]
63. Zhao, J.B.; Du, J.; Zhou, Q. Dry Layer of Soil below Artificial Forest near Xianyang in Shaanxi. *Sci. Geogr. Sin.* **2005**, *25*, 3322–3328.
64. Li, X.P.; Wang, L.; Guo, X.Y.; Chen, D.L. Does summer precipitation trend over and around the Tibetan Plateau depend on elevation? *Int. J. Climatol.* **2017**, *37*, 1278–1284. [CrossRef]
65. Lu, X.Y.; Kelsey, K.C.; Yan, Y.; Sun, J.; Wang, X.D.; Cheng, G.W.; Neff, J.C. Effects of grazing on ecosystem structure and function of alpine grasslands in Qinghai-Tibetan Plateau: A synthesis. *Ecosphere* **2017**, *8*. [CrossRef]
66. Zhang, P.; Zhang, L.; Chang, Y.; Xu, M.; Hao, Y.; Liang, S.; Liu, G.; Yang, Z.; Wang, C. Food-energy-water (FEW) nexus for urban sustainability: A comprehensive review. *Resour. Conserv. Recycl.* **2019**, *142*, 215–224. [CrossRef]
67. Fan, K.; Zhang, Q.; Singh, V.P.; Sun, P.; Song, C.; Zhu, X.; Yu, H.; Shen, Z. Spatiotemporal impact of soil moisture on air temperature across the Tibet Plateau. *Sci. Total Environ.* **2019**, *649*, 1338–1348. [CrossRef]